Materials and Design 192 (2020) 108747

Contents lists available at ScienceDirect

Materials and Design

journal homepage: www.elsevier.com/locate/matdes

Nanofibers with a tunable wettability by electrospinning and physical crosslinking of poly(2-*n*-propyl-2-oxazoline)

Ella Schoolaert [a], Luisa Cossu [a], Jana Becelaere [a], Joachim F.R. Van Guyse [b], Ali Tigrine [b], Maarten Vergaelen [b], Richard Hoogenboom [b,*], Karen De Clerck [a,*]

[a] Centre for Textile Science and Engineering, Department of Materials, Textiles and Chemical Engineering, Faculty of Engineering and Architecture, Ghent University (UGent), Tech Lane Science Park 70A, 9052 Ghent, Belgium

[b] Supramolecular Chemistry Group, Centre of Macromolecular Chemistry (CMaC), Department of Organic and Macromolecular Chemistry, Faculty of Sciences, Ghent University (UGent), Krijgslaan 281 S4, 9000 Ghent, Belgium

HIGHLIGHTS

- Poly(2-*n*-propyl-2-oxazoline) loses its thermoresponsive behavior in water at high concentrations
- Defined high molar mass poly(2-*n*-propyl-2-oxazoline) nanofibers are electrospun from an eco-friendly aqueous solvent system
- Nanofibers show thermoresponsivity, but can be stabilized by a simple, physical crosslinking procedure using tannic acid
- Altering tannic acid concentrations enables manipulation of membrane wettability, water uptake and rose-petal effect
- The membranes can be tuned from slowly absorbing water throug their pores to quickly spreading water across their surface.

GRAPHICAL ABSTRACT

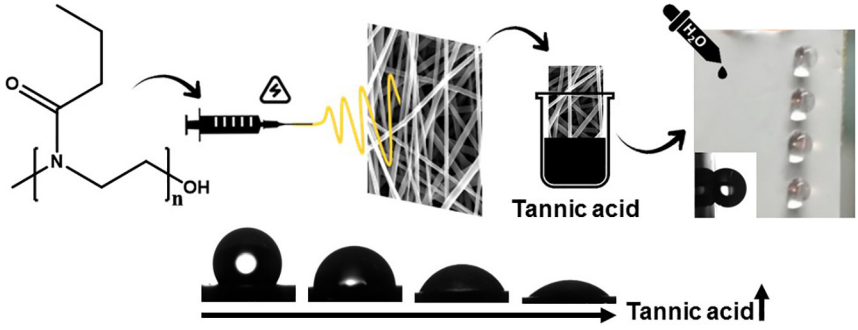

ARTICLE INFO

Article history:
Received 19 March 2020
Received in revised form 20 April 2020
Accepted 21 April 2020
Available online 24 April 2020

Keywords:
Poly(2-*n*-propyl-2-oxazoline)
Nanofibers
Wettability
Rose-petal
Contact angle
Tannic acid

ABSTRACT

This work shows the design of highly porous membranes with tunable wettability based on poly(2-*n*-propyl-2-oxazoline) (P*n*PrOx) nanofibers. Wicking and advanced contact angle experiments demonstrate the high potential for applications requiring specific interactions with aqueous media. P*n*PrOx is a popular member among the biocompatible poly(2-oxazoline)s due to its thermoresponsiveness in aqueous solutions, enabling the production of 'smart materials'. On material level, however, many interesting properties of this polymer remain undiscovered. Electrospinning is an ideal technique to transfer the properties observed in solutions to end-material properties, as the polymer is processed into highly porous, nanofibrous membranes. P*n*PrOx' electrospinnability is here investigated in environmentally friendly ethanol/water solvent systems, ensuring industrial scalability. The nanofibrous membranes show increased hydrophobicity exhibiting the rose-petal effect. Upon functionalization with tannic acid, the hydrophobic membranes are transformed into hydrophilic nanofibers showing water-stability in both fresh and salty water, even below the polymer cloud point temperature. By varying the tannic acid amount, the hydrophilicity can be fine-tuned as the contact area between water droplets and

* Corresponding authors.
E-mail addresses: richard.hoogenboom@ugent.be (R. Hoogenboom), karen.declerck@ugent.be (K. De Clerck).

https://doi.org/10.1016/j.matdes.2020.108747

surface, the rate and manner of water uptake and the extent of the rose-petal effect can be manipulated easily. Hence an interesting material is designed for applications in which water caption and transport are important.

1. Introduction

Poly(2-*n*-propyl-2-oxazoline) or P*n*PrOx is one of the members of the poly(2-oxazoline)s (PAOx), a class of polymers drawing increasing attention in a wide range of applications, especially in the biomedical field [1–7]. PAOx have been proposed as an alternative to commonly applied biomedical polymers such as poly(ethylene glycol), poly(N-isopropylacrylamide) and poly(N-vinylpyrrolidone) thanks to their biocompatibility [2,5,8], tunable solubility [1], size and structural variability [1,3], and straightforward chemical functionalization [9–13]. P*n*PrOx in particular is water-soluble and exhibits lower critical solution temperature (LCST) behavior, meaning that the polymer is soluble in water below its LCST, *i.e.*, ~25 °C, but insoluble above this temperature [1,14–18]. In the hydrated soluble state, P*n*PrOx shows excellent stealth behavior making this polymer and its copolymers ideal candidates for, *e.g.*, drug and gene delivery [1–5]. Apart from biomedical applications, the properties of P*n*PrOx are of interest to other fields as well, such as sensor applications and thermoresponsive systems [19–22].

With respect to these various fields of applications, nanofibers have been described extensively as a high-potential support material, being characterized by high porosity and high specific surface area thanks to the fine fiber diameter (below 500 nm) [23–30]. The membranes are typically produced by solvent electrospinning, which is a cost-efficient, straightforward and known production process in industry [27,29–31]. A large breakthrough of electrospinning on the market is, however, partially inhibited by the use of deleterious solvents needed to solubilize commonly applied hydrophobic polymers [31]. The use of water-soluble polymers, *e.g.*, thermoresponsive polymers, such as P*n*PrOx, can clear the way for a more environmentally friendly electrospinning process, therefore overcoming common barriers in electrospinning.

By combining the inherent properties of P*n*PrOx and nanofibers, an interesting thermoresponsive material can be designed that changes its behavior in aqueous environments depending on temperature, yet, this combination is scarcely investigated to date. Probably because extensive research towards both biomedical applications of PAOx and nanofibers has emerged only within the last two decades [8,32]. To the best of the authors' knowledge, no electrospinning of PAOx has been reported to this date, except for poly(2-ethyl-2-oxazoline) (PEtOx) and poly(2-isopropyl-2-oxazoline) and their copolymers [33–37].

In this work, a nanofibrous membrane with tunable wettability is created including the discovery of valuable and fundamental properties of P*n*PrOx. The electrospinnability and nanofiber properties of P*n*PrOx are investigated as well as the functionalization of the membranes with tannic acid. Well-defined P*n*PrOx of two different molar masses, *i.e.*, 30 kDa and 60 kDa, is applied to show the influence of molar mass on the P*n*PrOx thermoresponsivity and electrospinnability. The choice for tannic acid is twofold. First of all, tannic acid is applied as a biocompatible, physical crosslinking agent to solve the issue of water solubility below P*n*PrOx' LCST, which might be inconvenient for specific applications. Previous work already showed that water-instability of PEtOx nanofibers could be circumvented by crosslinking strategies, yet complex and requiring copolymers [34,35]. P*n*PrOx, on the other hand, allows for more straightforward crosslinking due to its more hydrophobic nature. Powerful hydrogen bonding is possible at the carbonyl groups of the present amides. Tannic acid has been applied before as a crosslinking tool based on its ability to form a high amount of hydrogen bonds at its galloyl moieties [38–43]. Crosslinking of PAOx nanofibers with tannic acid, however, has not been mentioned before.

The second reason to choose tannic acid as a functionalizing agent is that it provides hydrophilic entities to the material surface. As a result, the rather hydrophobic nature of the polymer nanofibers caused by their inherent surface roughness [44–51], can be altered to produce a material that is water-stable yet hydrophilic. Although electrospinning has frequently been used as a tool to produce superhydrophobic materials [47,50,52,53], hydrophilic nanofibrous materials that are water-stable might also be of great interest to many application areas where water caption and transport are important, *e.g.*, biomedical wound dressings.

Our work shows the applicability of a fundamental and important breakthrough in PAOx chemistry, being the synthesis of well-defined, high molar mass P*n*PrOx. By enabling the production of these longer polymers, they can be processed into valuable end-materials such as nanofibers since higher molar masses result in significant chain entanglement required for the formation of a continuous filament during processing. This work shows that well-defined P*n*PrOx can be successfully electrospun into a nanofibrous material with interesting surface properties. Importantly, the membranes can be produced by an ecological friendly and scalable electrospinning process as P*n*PrOx showed to be soluble in specific water/ethanol solvent systems at high concentrations. This is a benefit for biomedical applications as no toxic solvent rest fractions are present in the end-material. It is further shown that P*n*PrOx allows for stabilization in aqueous environments of different salinity by a simple crosslinking procedure using a biocompatible agent such as tannic acid. At the same time, the membrane's surface is functionalized enabling the manipulation of the surface wettability. Thanks to the easy-to-tune wettability, P*n*PrOx nanofibrous membranes could be of interest to all applications where water caption and transport are important, including filtration and biomedicine.

2. Experimental section

2.1. Materials

Ethanolamine (>99%) from Tokyo Chemical Industry (TCI), zinc acetate dihydrate and methyl-p-toluenesulfonate (98%) from Sigma-Aldrich, butyronitrile (>98.5%), ninhydrin, sodium and chlorobenzene (>99%) from Acros Organics were used as received unless stated otherwise. For the synthesis of 60 kDa P*n*PrOx chlorobenzene (Sigma-Aldrich) was sequentially washed three times with sulfuric acid (Sigma-Aldrich), sodium bicarbonate solution (Sigma-Aldrich) and deionized water. After drying over magnesium sulfate (Sigma-Aldrich) and barium oxide (Sigma-Aldrich), chlorobenzene was distilled twice under argon overpressure. 2-Phenyl-2-oxazoline (PhOx, Polymer Chemistry Innovation) was dried over barium oxide (Sigma-Aldrich) and distilled under vacuum. Tetrafluoroboric acid from Sigma-Aldrich was used as received. For the electrospinning solutions, mixtures of distilled water and absolute ethanol (99.8%, PanReac AppliChem) were applied. Physical crosslinking of nanofibers was done using tannic acid (1701.2 $g \cdot mol^{-1}$) from Sigma-Aldrich. All tests involving water were carried out with deionized water of type III as considered in ISO Standard 3696, having a conductivity below 0.5 $\mu S \cdot cm^{-1}$. To increase salinity of the aqueous solutions, NaCl (Sigma-Aldrich) was added to deionized water in different concentrations. The phosphate-buffered saline (PBS) solution was produced by adding 8 g of NaCl (Sigma-Aldrich),

0.2 KCl (Sigma-Aldrich), 1.44 g of Na_2HPO_4 (Sigma-Aldrich) and 0.24 g of KH_2PO_4 (Sigma-Aldrich) to 800 mL of deionized water. The pH of the mixture was adjusted to 7.4 by addition of HCl (Sigma-Aldrich). After reaching a pH of 7.4, deionized water was added until a volume of 1 L was reached. For water uptake tests a colored aqueous solution was made by addition of methylene blue (Sigma-Aldrich) to deionized water.

2.2. Synthesis of PnPrOx

PAOx are synthesized by cationic ring-opening polymerization of their respective 2-oxazoline monomers. In this work, P*n*PrOx of two different molar masses, *i.e.*, 30 kDa (M_n: 15300 $g \cdot mol^{-1}$, M_p: 26100 $g \cdot mol^{-1}$, Đ: 1.4, Figs. S1 and S2) and 60 kDa (M_n: 37400 $g \cdot mol^{-1}$, M_p: 51300 $g \cdot mol^{-1}$, Đ: 1.2, Figs. S1 and S2), were prepared which required different synthesis procedures to obtain well-defined polymers as chain transfer reactions become more pronounced at higher molar masses [54,55]. The synthesis procedures of both monomers and polymers are based on previous work [54–56], and details can be found in Supporting Information.

2.3. Electrospinning

Electrospinning solutions were prepared by dissolving different amounts of the polymers in water/ethanol solvent systems with different ratios expressed in volume percentage (vol%). Mass concentrations are expressed by weight percentages (wt%) defined as the ratio of polymer mass and the sum of polymer and solvent mass. Solvent electrospinning experiments were carried out using a mono-nozzle set-up with an 18 gauge Terumo mixing needle without bevel. A ring-electrode was mounted around the needle to efficiently guide the jet towards the collector, which enhanced process stability and reduced the deposition area giving thicker membranes. A stable Taylor cone was achieved at a flow rate of 0.5 $mL \cdot h^{-1}$, tip to collector distance of 15 cm and voltage between 15 kV and 25 kV at room conditions ((25 ± 5)°C and (35 ± 5)% relative humidity).

2.4. Physical crosslinking of the nanofibers

The produced nanofibrous membranes were physically crosslinked by dipping them in aqueous solutions of different tannic acid concentrations expressed in weight percentage (wt%) defined as the ratio of tannic acid to solution mass. The tannic acid concentration ranged from 0 wt% to 10 wt% which resulted in an increase in intensity of the orange-brown color of the dipping solutions. The dipping solutions were placed on a heating plate and a temperature of 30 °C was maintained during the crosslinking procedure. A dipping time of 10 s was chosen for all physical crosslinking treatments. The nanofibrous membranes were subsequently air-dried.

2.5. Characterization

Size Exclusion Chromatography (SEC) was performed on an Agilent 1260-series HPLC system equipped with a 1260 online degasser, 1260 ISO-pump, 1260 automatic liquid sampler (ALS), thermostatted column compartment (TCC) at 50 °C equipped with two PLgel 5 μm mixed-D columns and a precolumn in series, 1260 diode array detector (DAD) and a 1260 refractive index detector (RID). The used eluent was dimethylacetamide (DMA) containing 50 mM of LiCl at a flow rate of 0.5 mL/min. The spectra were analyzed using Agilent Chemstation software with the GPC add on. Molar mass and dispersity values were calculated based on PEtOx standards.

Gas chromatography (GC) was used to determine nitrile conversion during monomer synthesis and the monomer conversion during polymer synthesis as the ratio of the integrals respectively corresponding to the nitrile or monomer and the applied solvent dissolved in chloroform. The analysis was performed on an Agilent 7890A system equipped with a VWR Carrier-160 hydrogen generator and an Agilent HP-5 column of 30 m length and 0.32 mm diameter. An FID detector was used and the inlet was set to 250 °C with a split injection of ratio 25:1. Hydrogen was used as carrier gas at a flow rate of 2 mL/min. The oven temperature was increased with 20 °C/min from 50 °C to 120 °C followed by a temperature ramp of 50 °C/min to 300 °C.

^{1}H-Nuclear Magnetic Resonance (NMR) spectroscopic analysis was carried out with a Bruker Avance 300 MHz Ultrashield or a Bruker Avance II 400 MHz apparatus at room temperature. The samples were dissolved in deuterated chloroform (>99.8%, Eurisotop).

Cloud point temperature (T_{cp}) measurements were carried out by turbidimetry on an Avantium Crystal 16 turbidimeter. 1 mL of the solutions with different polymer concentrations was examined by cycling the temperature between 0 °C and 35 °C. The T_{cp} was determined as the temperature at which the transmission of the solution had lowered to 50% during heating. Following recent recommendations, the heating/cooling rate was set at 0.5 $K \cdot min^{-1}$ [57].

The viscosity of electrospinning solutions was calculated from flow curves measured on an MCR 302 Anton Paar rheometer with a Peltier CTD 180 heating equipment. 2 mL samples were pressed between a profiled, lower measuring plate and an upper, parallel rotating plate with a 25 mm diameter. Measurements were done at room conditions (25 °C, (35 ± 5)% relative humidity). Electrospinning processes are characterized by high shear rates. The shear rate was therefore logarithmically increased from 1 to 500 s^{-1}. Linear increase gave similar results. Newtonian behavior was observed for all solutions meaning that viscosity remains constant at all applied shear rates. Viscosity was calculated as the ratio of shear stress and shear rate.

All produced nanofibrous membranes were analyzed on an FEI Quanta 200 FFE Scanning Electron Microscope (SEM) at an accelerating voltage of 20 kV. Prior to analysis the samples were coated with gold using a sputter coater (Balzers Union SKD 030). The nanofiber diameters were measured using ImageJ software. The average diameters and their standard deviations were based on 50 measurements per sample.

Modulated temperature Differential Scanning Calorimetry (MDSC) was used to measure glass transition temperatures (T_g). A TA Instruments Q2000 equipped with a refrigerated cooling system (RCS90) was applied using nitrogen as purge gas (50 $mL \cdot min^{-1}$). The instrument was calibrated using Tzero technology for standard Tzero aluminum pans using indium at the heating rate applied during measurements. The heating rate was set at 2 $K \cdot min^{-1}$ and samples of (2.5 ± 0.5) mg were used. A temperature modulation of ±0.5 °C every 40 s was selected. Samples were subjected to two heating cycles from 0 °C to 250 °C. T_g was determined with TA Universal Analysis software.

Infrared (IR) spectra were recorded with a Fourier Transform Infrared (FTIR) spectrometer equipped with an Attenuated Total Reflectance (ATR) accessory (diamond crystal) from Thermo Scientific. Samples were excited with light of wavenumbers ranging from 4000 cm^{-1} to 400 cm^{-1}. A resolution of 4 cm^{-1} and 32 scans for each sample were applied.

UV–Vis spectra were recorded using a double beam Perkin-Elmer Lambda 900 UV–Vis spectrophotometer. Solutions were measured in transmission mode using 1 cm matched quartz cells while solid samples were characterized in reflection with an integrated Spectralon Labsphere (150 mm). The samples were excited with light of wavelengths ranging from 800 to 200 nm with a data interval of 1 nm for transmission and 4 nm for reflection. Transmission and reflection were converted into absorbance (A) and Kubelka-Munk (K-M) respectively.

The water stability of the nanofibrous membranes was tested by immersion of the membranes in deionized water at specific temperatures, *i.e.*, 5 °C (below the determined T_{cp}), 25 °C (around the determined T_{cp}) and 30 °C (above the determined T_{cp}), for times ranging from 10 min to 24 h. The membranes were subsequently dried in air. As physically

crosslinked membranes remain stable after 24 h, SEM-images of this immersion time are shown.

Stability of the membranes in aqueous solutions with increasing salinity (0.0017 M NaCl, 0.017 M NaCl, 0.17 M NaCl, 1.7 M NaCl, 5.1 M NaCl) as well as in PBS solution and regular tap water was investigated. Aqueous solutions were kept at 10 °C (below the determined T_{cp}) and samples were immersed overnight. Membranes were subsequently dried in air, SEM-images were taken.

Static and dynamic contact angles were determined with a DSA 30 Krüss GmbH drop shape analyzer and an OCA 25 contact angle setup with tilting base from DataPhysics. Droplets of 2 μL deionized water were dropped onto the nanofibers' surface at room conditions (25 °C, (35 ± 5)% relative humidity) and at 15 °C. Temperature regulation of samples and liquid could be achieved by using respectively a temperature chamber and a heating/cooling device for syringes. Average contact angles and standard deviations were measured using either ImageJ or OCA 25 software. Apart from static and dynamic contact angles, also the rose-petal effect was investigated by maximizing the droplet volume adhering to the sample surface when tilting the sample. Samples were always tilted at 2°/s. To evaluate the uptake of a water droplet by the membranes, a colored aqueous solution was used by dissolving methylene blue in deionized water.

3. Results and discussion

3.1. Solvent electrospinning and water stability of PnPrOx nanofibers

P*n*PrOx consists of a hydrophilic, tertiary amide based backbone with hydrophobic *n*-propyl groups in the side chains, which provides the polymer with thermoresponsive properties. Turbidimetry measurements indeed reveal cloud point temperatures (T_{cp}) ranging from 19 °C to 23 °C depending on the molar mass and concentration (Fig. S3), which is in agreement with literature [1,14,16,17]. P*n*PrOx is soluble in water below this temperature but phase separates above. A higher molar mass decreases the T_{cp} as the polymer chains become longer, which favors polymer-polymer interactions over polymer-water hydrogen bonds. This means that, already at lower temperature, it becomes thermodynamically more favorable to dehydrate the polymer chains as this process is entropy driven. For example, at a concentration of 10 mg·mL^{-1} the T_{cp} of P*n*PrOx of 30 kDa is 22 °C. On the other hand, the T_{cp} of P*n*PrOx of 60 kDa is 21 °C at the same concentration. Also polymer concentration has a significant influence on T_{cp}. Higher concentrations in water again benefit interchain interactions, reducing T_{cp}. However, true LCST behavior is not observed as the T_{cp} completely disappears if the concentration becomes too high, *i.e.* the polymer is no longer soluble/miscible with water at 150 mg·mL^{-1}. P*n*PrOx of these high molar masses thus becomes completely water-insoluble at high concentrations.

This phenomenon has a major influence on the production of P*n*PrOx nanofibers. Indeed, typically high polymer concentrations (>100 mg·mL^{-1} depending on molar mass) are required to induce sufficient chain entanglements for the formation of fibers. Since P*n*PrOx is not soluble in water at these high concentrations, water/ethanol solvent systems of different volumetric ratios (including 0/100 vol% water/ethanol) were chosen, which are still an environmentally friendly options. Hoogenboom et al. already described the solubility of P*n*PrOx in water/ethanol solvent systems, but only for low polymer concentrations, *i.e.*, 5 mg·mL^{-1} [14]. From Fig. 1 and Fig. S4 it is clear that at much higher concentrations relevant to the electrospinning process, *i.e.*, 250 mg·mL^{-1} for P*n*PrOx of 30 kDa and 150 mg·mL^{-1} for P*n*PrOx of 60 kDa, the polarity of the solvent system tremendously affects the solubility and, thus, the electrospinnability of P*n*PrOx. This can be explained by the combination of both hydrophilic and hydrophobic entities present in the polymer structure. The polarity of pure water and water containing up to 20 vol% of ethanol is too high resulting in complete insolubility of the polymer, which is reflected by zero transmittance during turbidimetry experiments. As the polarity of the solvent system decreases upon addition of more ethanol, the interchain interactions become less pronounced as more ethanol is present to interact with the hydrophobic sites of P*n*PrOx. Despite the suppression of interchain interactions by ethanol, they are still sufficiently present to induce phase separation. A gel-phase is formed which is separated from a second, liquid phase (Fig. 1a, 30 vol%–50 vol% ethanol in water). Depending on the vol% ethanol, the molar mass of the polymer and the polymer concentration, the transparency of the gel-phase changes. For solvent systems with up to 40 vol% of ethanol, the gels appear opaque as reflected by the zero transmittance during turbidimetry experiments. By further increasing the amount of ethanol to 50 vol% the gel-phase becomes transparent in a specific temperature window depending on the molar mass and concentration of the polymer, *e.g.*, between 6 °C and 30 °C for P*n*PrOx 30 kDa as determined by turbidimetry (Fig. 1b).

The transparency of the gel-phase is again linked to the polarity of the solvent system as an increase in solvent polarity enhances interchain interactions resulting in hydrophobic domains that scatter the light. These hydrophobic domains become less dense as the solvent system becomes less polar. This phenomenon can be visually observed as an increasing volume of gel-phase compared to liquid-phase as the vol % of ethanol in the solvent system increases (Fig. 1a and Fig. S4). In other words, a less polar solvent system allows for the polymer chains to be more extended resulting in the transparent gel-phase. By further decreasing the polarity of the solvent system upon addition of an excess

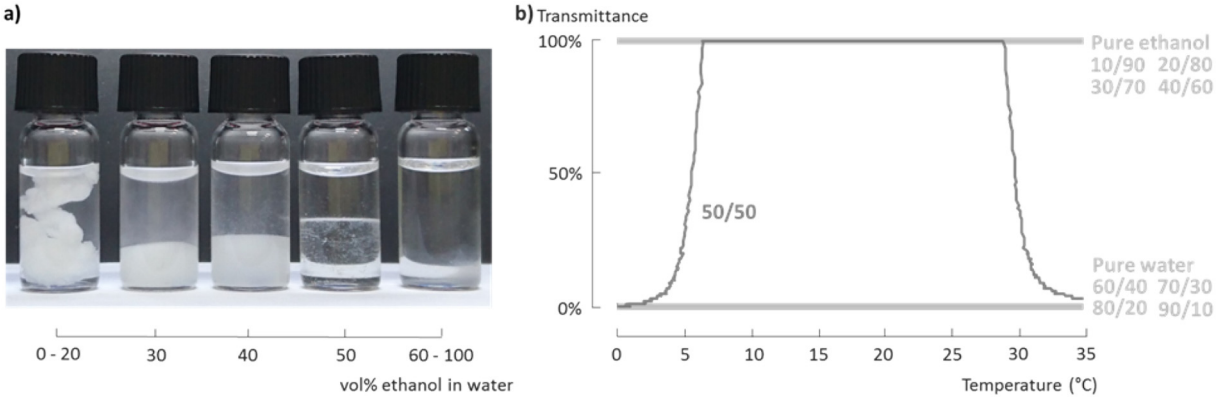

Fig. 1. a) Pictures and b) turbidimetry analysis of P*n*PrOx of 30 kDa (250 mg·mL^{-1}) in water/ethanol solvent systems with different ratios show that, as the polarity of the solvent system decreases, *i.e.*, vol% ethanol increases, the polymer solution changes from phase separated over an opaque gel and a transparent gel to eventually a clear solution. In solvent systems with 30 vol% to 50 vol% ethanol, the gel phase increases in volume as the polarity of the solvent system decreases (a). From 60 vol% onwards, the polymer is completely soluble in the water/ethanol solvent system (note that the vial on the right contains a stirring bar). In (b) the solvent ratio is depicted as x/y with x the vol% of water and y the vol% of ethanol.

of ethanol, *i.e.*, >60 vol%, complete dissolution of P*n*PrOx is achieved without gel formation. Indeed, 100% transmittance is observed during turbidimetry measurements, representing clear, electrospinnable solutions for 40/60, 30/70, 20/80 and 10/90 water/ethanol solvent systems. In pure ethanol, heating is required to fully dissolve the polymer, which may be attributed to weaker interactions between the P*n*PrOx and ethanol compared to water, leading to slower dissolution in absence of water.

Based on these observations the 0/100, 10/90, 20/80, 30/70 and 40/60 water/ethanol solvent systems are selected to perform optimization of the electrospinning process. Electrospinning from pure ethanol results in a rather unstable process due to high volatility of the solvent. All other solvent systems result in nanofiber diameters between 200 and 400 nm, however 30/70 and 20/80 water/ethanol combinations were found to give the most stable process (Fig. 2). As expected, viscosity increases significantly with increasing polymer concentration (Figs. S5 and S6). The nanofiber diameter follows this trend until uniform, bead-free nanofibers are obtained at concentrations of 35 wt% and 25 wt% for P*n*PrOx 30 kDa and 60 kDa, respectively (Figs. S5 and S6). The need for a lower polymer concentration at higher molar mass is explained by the increase in chain entanglements with increasing molar mass, which is a typical observation in electrospinning and was also observed for solvent electrospinning PEtOx [27–30,33]. What is also apparent for P*n*PrOx 60 kDa, is the increase in viscosity and therefore nanofiber diameter as the water content in the solvent system increases (Fig. S6). As water is a poor solvent for P*n*PrOx, polymer-polymer interactions are strengthened resulting in higher solution viscosity, which is most pronounced for P*n*PrOx with the highest molar mass. The ability to electrospin different P*n*PrOx concentrations and molar masses brings the opportunity to play with process parameters and design specific nanofiber morphologies, *e.g.*, fiber diameters.

Like the bulk material, produced P*n*PrOx nanofibers exhibit thermoresponsive behavior. The membranes are completely unstable and dissolve in water below the determined T_{cp} values, *i.e.*, 19 °C–23 °C, yet the membranes do not dissolve nor swell above these threshold temperatures and they show remarkable surface properties (Fig. S7). Both above and below the determined T_{cp} values, nanofibrous membranes show an initial contact angle of (119 ± 6)° (Figs. S8 and S19). The nanofibrous surface is therefore much more hydrophobic compared to thin films of the same polymers having contact angles of only (80 ± 10)°. Electrospinning polymers into nanofibers has extensively been reported before to lead to an increase in the hydrophobicity of material surfaces, which is of great interest for applications such as self-cleaning and responsive smart materials, microfluidics, filtration and biomedicine [44–51,58,59]. Increased hydrophobicity arises from the inherent roughness of nanofibers created by their small diameter and porous structure. This characteristic allows the surface to entrap air, which is one of the most important factors next to the surface chemistry of the applied materials, to determine hydrophobicity of a surface according to the Cassie-Baxter theory [60,61]. In case of P*n*PrOx nanofibers, both requirements are likely to be fulfilled. The polymer itself provides hydrophobicity by the presence of apolar segments (alkyl side chains) and the nanofibrous structure provides the required surface roughness, resulting in high contact angles and hydrophobic properties [61].

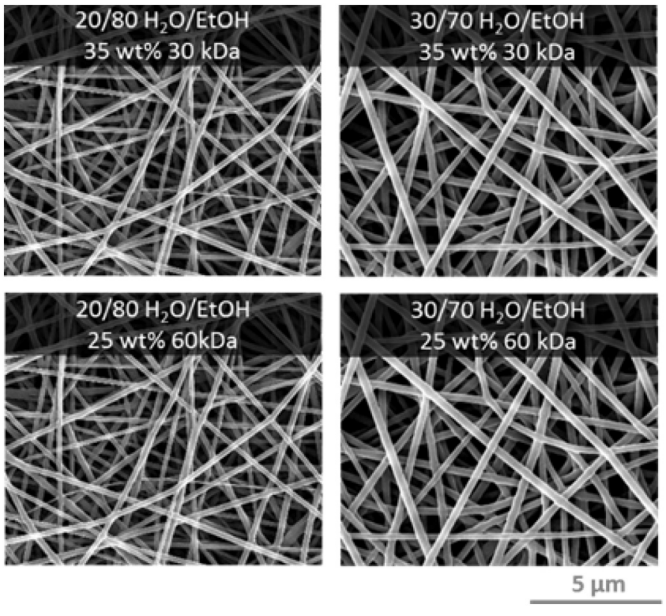

Fig. 2. SEM images of nanofibers based on 30 kDa (top) and 60 kDa (bottom) P*n*PrOx solutions show good electrospinnablity from water/ethanol solvent systems.

On top of the thermoresponsive solubility in deionized water, it is important to investigate stability in other aqueous environments as well. Depending on the foreseen biomedical applications, the produced P*n*PrOx nanofibers may likely come into contact with aqueous solutions of different salinity. In previous studies it was already shown that specific salts, such as NaCl, act as Hofmeister salts for P*n*PrOx, thereby decreasing the cloud point temperature in aqueous solutions with increasing salt concentration [62]. Based on immersion of the nanofibrous membranes in aqueous solutions with different NaCl concentrations, it is here concluded that this salting out effect can be extended to the P*n*PrOx nanofibers. From Fig. S9 it is clear that the stability of the P*n*PrOx nanofibers below 20 °C increases with water salinity. In solutions that are rather salty, P*n*PrOx nanofibers are completely stable. This means that the P*n*PrOx nanofibrous membranes remain intact when in contact with physiological fluids, such as phosphate-buffered saline (PBS) or sea water, which might be of interest to real-life applications. In fresh water, such as deionized and typical tap water, however, the membranes dissolve at 10 °C. Physical crosslinking of the membranes will here be necessary to stabilize the membranes.

3.2. Physical crosslinking of PnPrOx nanofibers

To improve water stability of the P*n*PrOx nanofibers in fresh water, the membranes were physically crosslinked by dipping them in aqueous solutions with varying tannic acid concentrations. As P*n*PrOx nanofibers are soluble in water below the polymer's T_{cp} (20 °C), membranes are immersed in tannic acid solutions at 30 °C. This is above the T_{cp}, but below the T_g of P*n*PrOx to preserve the nanofiber's integrity (Fig. S10). As can be seen from Fig. 3, the crosslinking process does not alter the nanofiber morphology (more SEM images can be found in Figs. S11 and S12). However, note that at higher tannic acid concentrations, *e.g.*, 3%–4%, film formation starts between the nanofibers, which merges into an entire film covering the membrane's surface at very high tannic acid concentrations, *i.e.*, 5%–10%. At high concentration, tannic acid is capable of intermolecular hydrogen bonding between its galloyl moieties leading to formation of a film on the substrate's surface. This is also visually observed as a shiny layer on the otherwise matte surface of the nanofibrous membranes (Fig. S13).

If the tannic acid concentration is limited, *e.g.*, 0.1%–2%, the galloyl moieties preferentially form hydrogen bonds with the carbonyl groups of P*n*PrOx as depicted in Fig. 4a, thereby crosslinking the nanofibers. The driving force for this process is the strong hydrogen bonding interaction between the carbonyl groups of the PAOx polymers (acceptor) and the phenolic hydroxyl groups of tannic acid (donor) [39–41,43]. No film or aggregates are then observed, indicating that the tannic acid is well distributed among the P*n*PrOx polymer chains.

IR and UV–Vis spectra of the physically crosslinked nanofibers clearly show peaks from both components and the relative intensities of the IR peaks corresponding to tannic acid increase with tannic acid concentration applied during the crosslinking process, confirming the

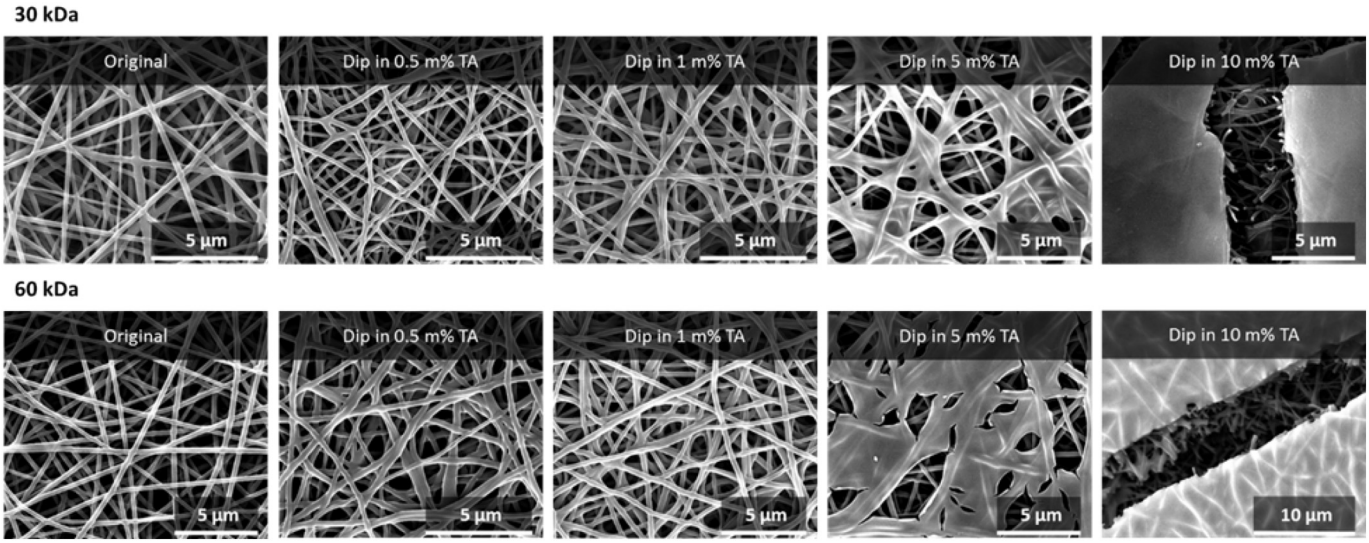

Fig. 3. SEM images of nanofibrous membranes after immersion in aqueous solutions of varying tannic acid concentration show that the nanofiber integrity remains intact. At high tannic acid concentrations a film is formed on the surface of the nanofibrous membranes.

presence of tannic acid in the nanofibrous membranes (Figs. 4b and 5). The formation of hydrogen bonds, *i.e.*, crosslinks, between the polymer and tannic acid is reflected by a shift of the peak corresponding to the C═O stretching vibration of P*n*PrOx (1639 cm^{-1}) towards lower wavenumbers (1627 cm^{-1}) in the IR spectra (Fig. 5) and by the shift of the tannic acid peaks at 210 nm and 275 nm and the appearance of two additional peaks at 235 nm and 300 nm in the UV–Vis spectra (Fig. 4b) [63–67]. The latter phenomenon indicates that tannic acid is present in two different forms being its neutral form, represented by the peak maxima at 210 and 275 nm, and its phenolate or ionized form, represented by the peak maxima at 235 nm and 300 nm [65–67]. The peak maxima of the phenolate form are bathochromically shifted with respect to the peak maxima of the neutral form as a result of the larger delocalization of non-binding electrons. The shift of the peak at 1700 cm^{-1} towards higher wavenumbers and the broadening of the peak corresponding to —OH around 3300 cm^{-1} in the IR spectra further confirm the presence of inter- and/or intramolecular hydrogen bonds of tannic acid molecules.

A spectral representation of the formation of the tannic acid film on the surface of the nanofibrous membranes visualized by SEM analysis is also apparent from the IR and UV–Vis spectra as the spectrum of tannic acid completely overlaps with the spectrum of P*n*PrOx at high tannic acid concentrations, *i.e.*, 5%–10%. For instance, the peak maxima of P*n*PrOx at 1460 cm^{-1} and 1428 cm^{-1} slowly get overshadowed by the peak maximum of tannic acid around 1443 cm^{-1} with increasing concentration. In UV–Vis spectroscopy the peak corresponding to the neutral form of tannic acid at 275–280 nm is hypsochromically shifted to 260 nm as the amount of tannic acid increases to 10%. At the same time the additional peak at 300 nm corresponding to tannic acid's phenolate form becomes more pronounced by bathochromically shifting to 330 nm. Additionally, the peaks at 210 nm and 235 nm seem to disappear, suggesting that the peak maxima at 235 nm for tannic acid concentrations up to 4% arise from the specific hydrogen bond interactions between P*n*PrOx and tannic acid.

The formation of hydrogen bonds between P*n*PrOx and tannic acid significantly enhance the stability of the nanofibrous membranes in water with limited salinity. Whereas pure P*n*PrOx nanofibers dissolve in fresh water at temperatures below 20 °C, Fig. 6 clearly demonstrates that the physically crosslinked nanofibers remain stable for at least 24 h in all aqueous environments, including deionized water, tap water and PBS (more SEM images can be found in Figs. S15 and S16). Depending on the tannic acid concentration, different behavior is observed. Membranes that are crosslinked with low tannic acid concentrations, *e.g.*, 0.1%–0.5%, show a mechanical response while preserving their nanofiber integrity. The membranes shrink during the tests due to the limited amount of physical crosslinks combined with water absorption. Membranes that are crosslinked with higher tannic acid concentrations are dimensionally stable when immersed in water.

UV–Vis and IR spectroscopy following the water stability tests confirm that P*n*PrOx and tannic acid are both still present and hydrogen bonds are established between both components (Figs. S17 and S18). The tannic acid film formed on the membrane's surface during the crosslinking procedure with high tannic acid concentrations, *e.g.*, 5%–10%, has disappeared after water immersion (Figs. S15 and S16) and the otherwise by the film overshadowed IR and UV–Vis spectra now resemble the spectra of nanofibers crosslinked with lower tannic acid concentrations, *e.g.*, 1% (Figs. S17 and S18). By immersion in water the film is simply washed away leaving water-stable nanofibers behind. Indeed, in IR spectroscopy for instance, the peak maxima at 1639 cm^{-1} representing the C═O stretching vibration of P*n*PrOx have clearly shifted to approximately 1625 cm^{-1} as was also the case for nanofibers crosslinked with low tannic acid concentrations, confirming the presence of hydrogen bonds between polymer and tannic acid.

Interestingly, the presence of nanoparticles was observed after the water solubility tests in some cases. This phenomenon could be explained by the presence of an excess amount of tannic acid. By immersion in water, most of this excess is removed, *i.e.*, film is washed away, yet some aggregates of tannic acid may be formed on the P*n*PrOx substrate based on intermolecular hydrogen bonding.

3.3. Tannic acid provides tunable wettability

In addition to successfully crosslinking and thereby stabilizing P*n*PrOx nanofibers in different aqueous environments at all temperatures, tannic acid provides interesting functionality to the membrane surface. As previously described, the non-crosslinked P*n*PrOx nanofibers show rather hydrophobic surface properties as reflected by a high contact angle. However, for many applications where nanofibers are investigated for, a water-stable yet hydrophilic membrane could be of interest, *e.g.*, biomedical haemodialysis [74]. Tannic acid adds many hydrophilic groups to the nanofibrous surface (Fig. 4a), which influences the surface wettability of the membranes. Indeed, the initial contact angle decreases drastically after physical crosslinking with tannic acid, regardless of temperature and water salinity (Fig. 7a, Figs. S19, S21,

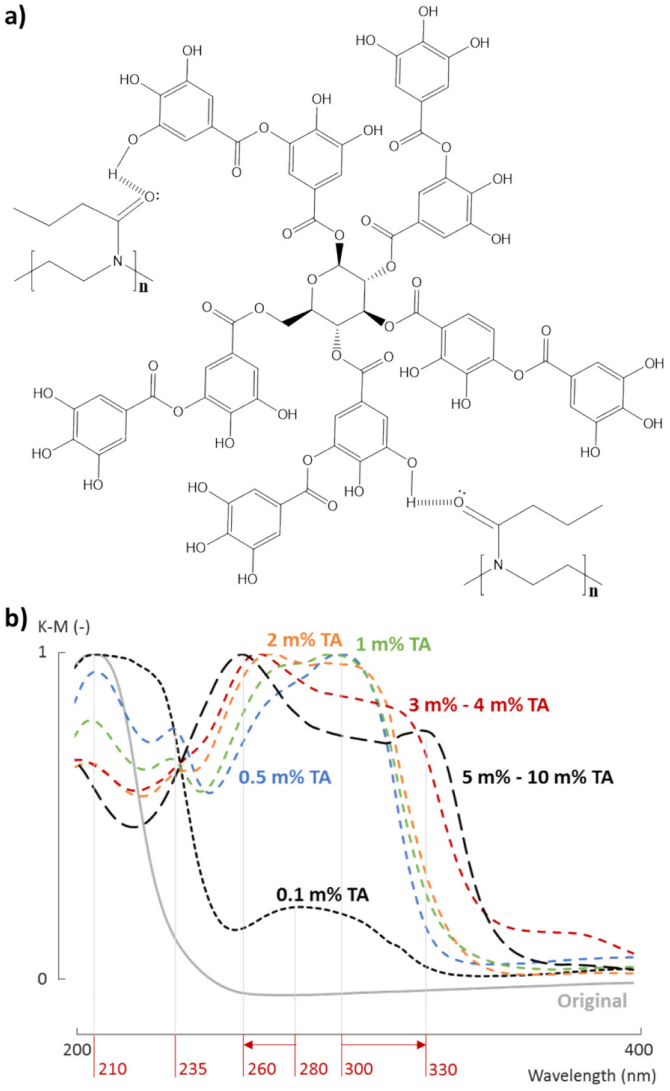

Fig. 4. a) Schematic representation of hydrogen bonds created during physical crosslinking between the hydroxyl groups of the galloyl moieties of tannic acid and the carbonyl groups of the amides belonging to P*n*PrOx. b) UV–Vis spectroscopy of crosslinked nanofibers show additional peak maxima arising from the presence of tannic acid's phenolate form, indicating the presence of hydrogen bonds (210 nm: combined absorption of the amide groups of P*n*PrOx and the $\pi \rightarrow \pi^*$ transition of tannic acid [63,64], 275–280 nm: absorption of phenyl groups of tannic acid (Fig. S14) [63,65–67]).

Movies 1, 2 and 3). Additionally, the contact angle can now be further tuned over a range of 50° by altering the tannic acid concentration during the crosslinking procedure (Fig. 7a). This allows the transformation of a rather hydrophobic nanofibrous membrane into a tunable hydrophilic membrane simply by dipping the membrane in aqueous solutions with different tannic acid concentrations. In the original, non-crosslinked, P*n*PrOx nanofibers, the contact angle slowly decreases after initial contact between the water droplet and the nanofibrous surface as the droplet gets absorbed by the membrane (Fig. 7b and Movie 1). The speed of this water uptake can be manipulated by changing the temperature as the droplet gets absorbed much faster at 10 °C compared to 25 °C. This is because P*n*PrOx is more sensitive to water below its cloud point temperature. Eventually, at low temperatures the membrane is dissolved, whereas the membrane remains intact at higher temperatures.

If the P*n*PrOx nanofibers are then crosslinked upon addition of tannic acid, the membranes are not only protected from dissolution, the water uptake after initial contact between the water droplet and the crosslinked membrane is also significantly faster both below and above the T_{cp} of the original P*n*PrOx (Fig. 7b).

Further analysis of the wetting behavior reveals that tannic acid not only allows for manipulation of the contact angle and the speed of water uptake, but also enables an entirely different behavior of droplet absorption. Fig. S20 illustrates how a colored water droplet is fully absorbed in only 20 min compared to 1 h by respectively a crosslinked and a non-crosslinked membrane. In addition, the colored water droplet does not migrate through a crosslinked membrane. It is rather spread across the surface and does not reach the back of the membrane. This is in great contrast with the non-crosslinked samples, in which the colored water is not spread over the sample surface. It is rather locally absorbed and penetrates through the membrane all the way to the back of the sample. The membrane even seems to shrink a bit as a consequence of the membrane absorption. SEM images prove that for both crosslinked and non-crosslinked samples, the nanofibrous structure is not damaged by the absorption of the water droplet at room temperature (Fig. S22). This behavior is observed for both fresh and salty water (Figs. S20 and S21), indicating that the surface wettability is altered by the tannic acid. So, without tannic acid, P*n*PrOx nanofibers are a rather hydrophobic material with low wettability, *i.e.*, high contact angle. A water droplet is not spread across the surface but is taken up slowly as it penetrates through the membrane, destroying the nanofibrous structure depending on temperature, *i.e.*, above or below T_{cp}. When tannic acid is present, a hydrophilic yet water-stable membrane is created, showing good wettability when in contact with a water droplet, *i.e.*, low contact angle, which is completely and quickly taken up by spreading it across the surface. By simply dipping the P*n*PrOx nanofibers in tannic acid solutions, a completely different and tunable behavior towards water can thus be achieved. This might be of interest to specific applications. For example, for water-based filtration processes it was shown that a hydrophilic layer increases the water flux and reduces incomplete wetting and fouling of a composite membrane filter [75–79]. Also for biomedical filtration, haemodialysis, hydrophilic surfaces are beneficial [74]. Furthermore, the procedure allows for the functionalization of only one of the two membranes' surfaces, resulting in a material with a hydrophobic surface at one side and a hydrophilic surface at the other side. An interesting material can thus be designed with high potential for many applications that require specific interactions with aqueous media.

So far, the membranes were always handled horizontally. But also when held vertically or upside down, P*n*PrOx nanofibrous membranes show interesting wetting behavior that is tunable upon addition of tannic acid. The P*n*PrOx nanofibrous membranes, both non-crosslinked and crosslinked, were found to exhibit the so called rose-petal effect. This effect is known as the phenomenon where an aqueous droplet remains spherical without rolling off the surface. Instead, the droplet attaches to the surface even when the membranes are held upside down (Fig. 8 and Movie 4) [61,80–82].

This phenomenon is ascribed to the presence of both micro-and nanoscale roughness on the P*n*PrOx nanofibrous surface. The roughness on nanoscale causes the high static contact angle whereas the roughness on microscale shows such low density and height allowing water to partially penetrate into the microstructure which results in high water adhesion [50,61,80–82]. The same effect was also recently observed in a few other nanofibrous systems by various authors and could again be interesting for many applications such as filtration, microfluidics, sensors and catalysis [50,83–85]. Especially because the end-material is rarely used in horizontal position in these kind of applications, high water adhesion is beneficial to promote contact of the material with the aqueous phase.

The rose-petal effect was further characterized by measuring the dynamic contact angles during tilting of the samples. Advancing and receding contact angles were measured and contact angle hysteresis was calculated for different droplet volumes (Table S1). The maximum

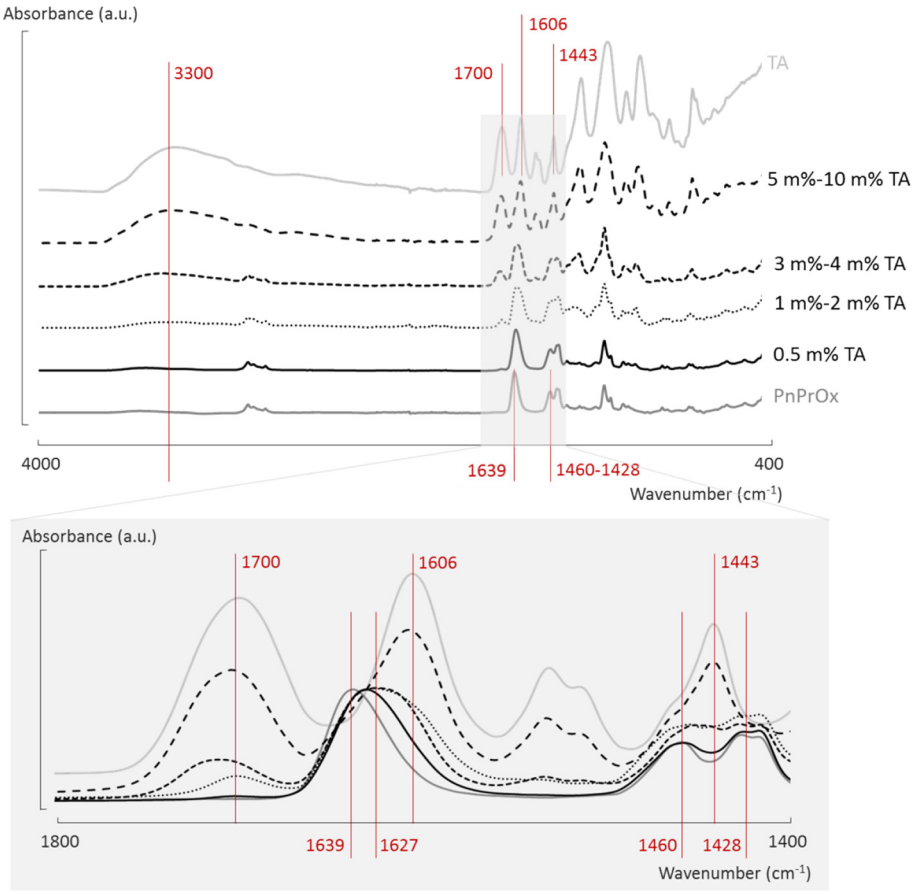

Fig. 5. IR spectra reveal the presence of tannic acid in the physically crosslinked nanofibers as well as the presence of hydrogen bonds between P*n*PrOx and tannic acid (1639 cm^{-1}: C═O stretching vibration of P*n*PrOx [64,68–70], 1460 cm^{-1} and 1428 cm^{-1}: alkane entities of P*n*PrOx [64,68–70], 1700 cm^{-1}: C═O stretching vibration of tannic acid [68–73], 1606 cm^{-1}: C—O vibration of tannic acid [68–73], 1443 cm^{-1}: —C—C aromatic vibration of tannic acid [68–73]).

droplet volume that could stay attached to the membrane without rolling off, was determined. If the droplet did not roll off in vertical position, *i.e.*, at 90° tilt, the left and right contact angle were measured as the receding and advancing contact angle respectively. When the maximum volume was crossed and the droplet did roll off the sample surface, the receding and advancing contact angles were determined at the tilt angle just before the droplet started to roll off.

From Fig. 9 and Table S1 it is clear that not only the original P*n*PrOx nanofibers exhibit the rose-petal effect. Upon physical crosslinking of the membranes with tannic acid, the rose-petal effect is preserved, although the attachment of the droplet to the surface is again somewhat different due to the hydrophilic entities that tannic acid introduces to the surface. Indeed, the dynamic contact angles are lower if the membranes are crosslinked with tannic acid, as was also the case for the static contact angles. Moreover, the maximum volume that stays attached to the surface in vertical position is only 20 μL compared to 30 μL in case of non-crosslinked membranes. At the same droplet volume, the tilt angle needed to initiate rolling is lower, *e.g.*, 34° for a 1 m % TA crosslinked membrane compared to 53° for a non-crosslinked membrane (Table S1 and Movie 5). This could be ascribed to the higher

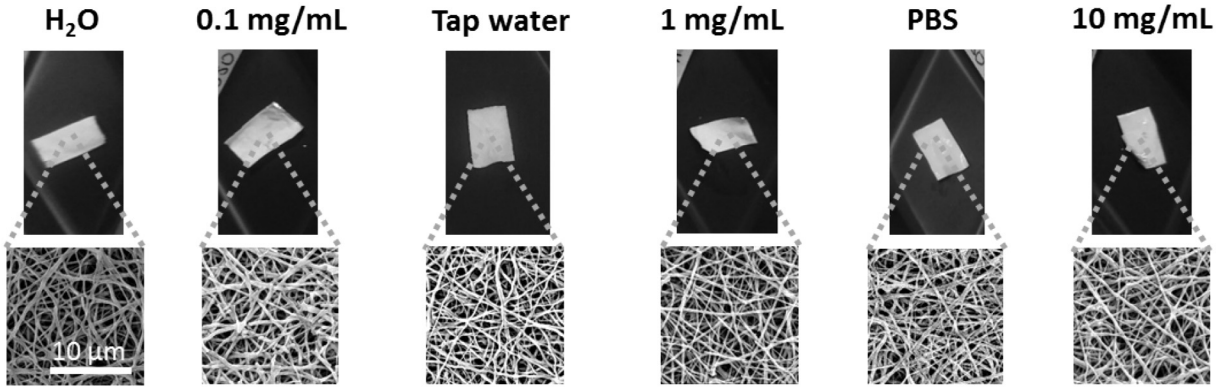

Fig. 6. Pictures and SEM images of physically crosslinked P*n*PrOx 30 kDa nanofibers (1 m% TA) after water stability tests in aqueous solutions with different NaCl concentrations at 5 °C. Compared to non-crosslinked P*n*PrOx nanofibers, physically crosslinked nanofibers remain intact in water with low salinity, so called fresh water, such as deionized and tap water.

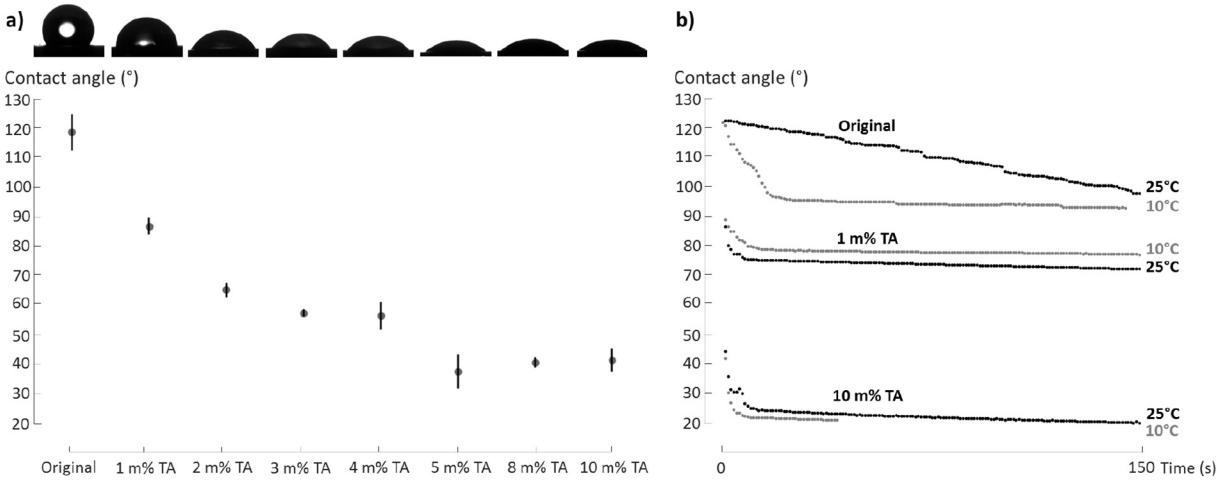

Fig. 7. a) Initial contact angles in function of amount of physical crosslinking clearly show that non-crosslinked nanofibrous membranes show the highest contact angle. Physically crosslinked membranes show a much lower initial contact angle which decreases further with increasing tannic acid concentration applied during the crosslinking procedure. b) Contact angles of a water droplet on a P*n*PrOx 30 kDa nanofibrous membrane in function of time show that contact angles decrease as the water droplet is slowly taken up by the membrane. At lower temperatures, *e.g.*, 10 °C, the water uptake is faster in case of the original, non-crosslinked membranes due to its water sensitivity below its T_{cp}. For crosslinked membranes, *e.g.*, with 1 m% and 10 m% tannic acid, the water uptake is even faster than for the original membranes, regardless of temperature.

water affinity of the surface if tannic acid is present, leading to easier spreading of the water droplet. So, the extent of the rose-petal affect can be altered by the introduction of tannic acid on the nanofibrous surface. Note that the advancing contact angles are similar to the previously observed static contact angles and remain more or less similar for different droplet volumes. The receding contact angles, on the contrary, decrease with increasing droplet volume as the heavier, larger droplets weigh down under gravity. This in turn results in larger contact angle hysteresis if larger droplet volumes are applied (Table S1).

4. Conclusions

Despite its interesting properties, particularly for biomedicine, the design of P*n*PrOx end-materials, including membranes, is still scarcely investigated. In this work, electrospinning and further characterization of P*n*PrOx nanofibrous membranes has been explored for the first time, resulting in an important contribution to the knowledge, applicability and potential of PAOx nanofibers in general.

It is shown that P*n*PrOx' thermoresponsivity highly depends on the polymer concentration. The polymer is not soluble in water at the high concentrations that are required for solvent electrospinning. Therefore, environmentally friendly water/ethanol solvent systems have been investigated, showing that well-defined P*n*PrOx of both 30 kDa and 60 kDa can be electrospun if at least 60 vol% ethanol is present. Uniform, beadless nanofibers are obtained that show the typical thermoresponsive behavior of the polymer in fresh water. In salty water, such as PBS and sea water, the nanofibers are completely stable at all temperatures.

A straightforward physical crosslinking procedure based on dipping the nanofibrous membranes in aqueous tannic acid solutions is proposed to circumvent the instability in fresh water below 20 °C. Tannic acid further provides the P*n*PrOx nanofibers with additional surface functionality as it introduces hydrophilic entities to the membrane surface, thereby creating a water-stable yet hydrophilic material. By changing the applied amount of tannic acid, P*n*PrOx nanofibers could be changed from being a hydrophobic material that slowly absorbs a water droplet throughout the pores of the membrane to a hydrophilic material that quickly spreads a water droplet across its surface. As crosslinked membranes showed higher affinity for water droplets, also the extent of the rose-petal effect could be manipulated in such way that water droplets roll off easier or at a smaller droplet volume. Further research includes the design of a multilayer material where only one side of the nanofibrous membrane is functionalized with tannic acid, offering different surface properties on either sides of the membrane.

This work shows that a popular member of the PAOx group, P*n*PrOx, can be processed into nanofibers in a straightforward and ecological friendly way, allowing, by simply dipping in tannic acid solutions, the design of its surface wettability characteristics to match the end-users wishes. It is without doubt that P*n*PrOx nanofibers are an interesting material with an easy-to-tune functional surface architecture, which might be of great interest to both chemistry and material sciences to develop advanced applications in various fields where water caption and transport are important, including biomedicine.

Synthesis procedure for monomers and polymers (PDF); ^{1}H NMR-spectra of the synthesized polymers (PDF); SEC-traces of the synthesized polymers (PDF); Cloud point temperatures of P*n*PrOx 30 kDa and 60 kDa (PDF); Pictures and turbidimetry analysis of P*n*PrOx 60 kDa (PDF); SEM images of P*n*PrOx 30 kDa nanofibers electrospun from different water/ethanol solvent systems (PDF); SEM images of P*n*PrOx 60 kDa nanofibers electrospun from different water/ethanol solvent systems (PDF); SEM images of nanofibers immersed in water at 25 °C and 30 °C (PDF); Pictures of a water droplet on a P*n*PrOx film and P*n*PrOx nanofibers (PDF); MDSC traces of P*n*PrOx (PDF); SEM images of physically crosslinked P*n*PrOx 30 kDa nanofibers after dipping

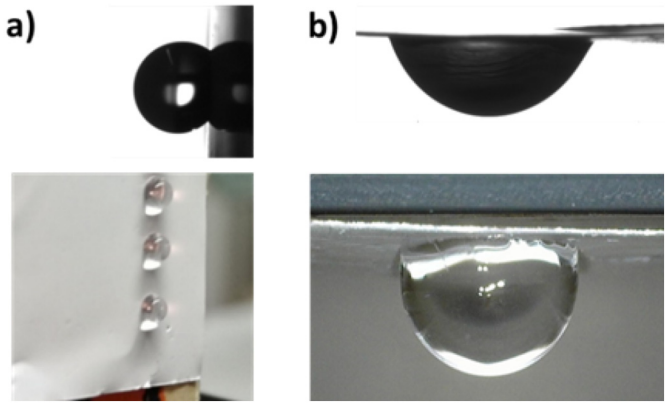

Fig. 8. Visualization of the rose-petal effect. a) Water droplets of 2 μL attach to the nanofibrous surface without rolling off when held vertically. b) Also higher droplet volumes, *e.g.*, 20 μL stay attached to the nanofibrous surface, even when held upside down.

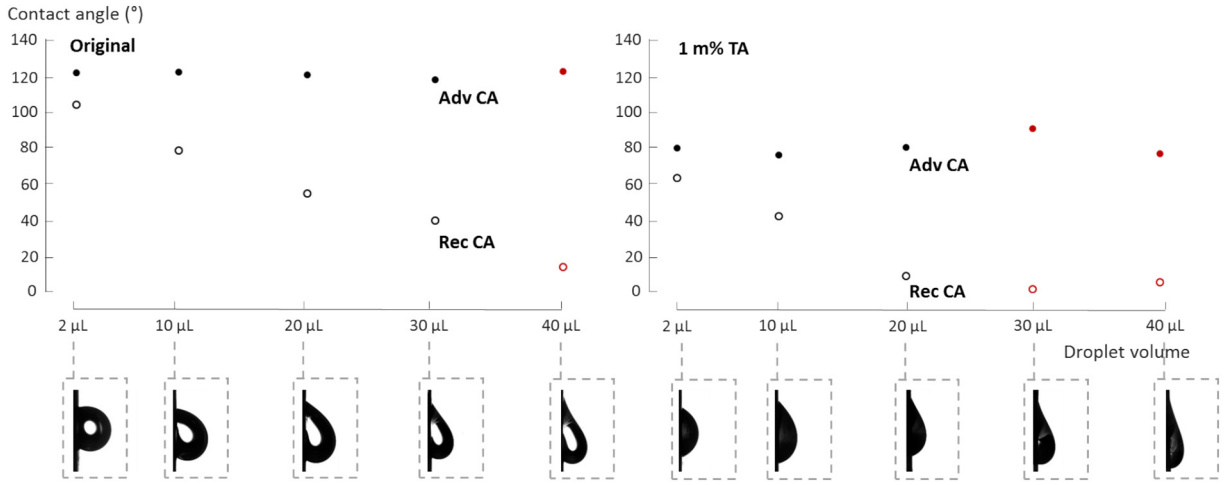

Fig. 9. Advancing and receding contact angles (Adv CA and Rec CA) at a tilt of 90° for a non-crosslinked P*n*PrOx 30 kDa nanofibrous membrane (left) and a 1 m% TA crosslinked P*n*PrOx 30 kDa nanofibrous membrane (right) at different droplet volumes. Advancing contact angles (filled dots) seem to be similar for different droplet volumes whereas receding contact angles (empty dots) decrease with increasing droplet volume. The red dots represent the volumes at which the droplet rolled off during tilting. This occurred at a tilt of 53° with a 40 µL droplet for the non-crosslinked membrane and at a tilt of 60° or 34° for the crosslinked membranes with 30 µL and 40 µL respectively.

in tannic acid solutions (PDF); SEM images of physically crosslinked P*n*PrOx 60 kDa nanofibers after dipping in tannic acid solutions (PDF); Pictures of nanofibrous membranes after physical crosslinking (PDF); UV–Vis spectrum of tannic acid (PDF); SEM images of physically crosslinked P*n*PrOx 30 kDa nanofibers showing water stability (PDF): SEM images of physically crosslinked P*n*PrOx 60 kDa nanofibers showing water stability (PDF); UV–Vis spectroscopy before and after the water stability tests (PDF); IR spectroscopy before and after the water stability tests (PDF); Initial contact angles of non-crosslinked and crosslinked P*n*PrOx 30 kDa nanofibrous membranes at 10 °C (PDF); Pictures of a fresh water droplet on crosslinked and non-crosslinked P*n*PrOx 30 kDa nanofibrous membranes (PDF); Pictures of a salty water droplet on crosslinked and non-crosslinked P*n*PrOx 30 kDa nanofibrous membranes (PDF); SEM images of non-crosslinked and crosslinked P*n*PrOx 30 kDa nanofibrous membranes after absorption of a colored water droplet at room temperature (PDF); Table with dynamic contact angles in function of droplet volume determined by tilting crosslinked and non-crosslinked P*n*PrOx 30 kDa nanofibrous samples (PDF); Movie showing the slow uptake of a water droplet by a P*n*PrOx 30 kDa nanofibrous membrane (AVI); Movie showing the fast initial decrease in contact angle when a water droplet touches a 1 m% TA crosslinked P*n*PrOx 30 kDa nanofibrous membrane (AVI); Movie showing the fast initial decrease in contact angle when a water droplet touches a 10 m% TA crosslinked P*n*PrOx 30 kDa nanofibrous membrane (AVI); Movie showing the rose-petal effect as a P*n*PrOx 30 kDa nanofibrous membrane is tilted from 0° to 90° (AVI); Movie showing a water droplet, which crossed the maximum volume for the rose-petal effect, rolling off a P*n*PrOx 30 kDa nanofibrous membrane tilted from 0° to the roll off angle (AVI). Supplementary data to this article can be found online at https://doi.org/10.1016/j.matdes.2020.108747.

CRediT authorship contribution statement

Ella Schoolaert: Conceptualization, Methodology, Validation, Formal analysis, Investigation, Writing - original draft, Writing - review & editing, Visualization. **Luisa Cossu:** Validation, Formal analysis, Investigation. **Jana Becelaere:** Formal analysis, Investigation, Writing - review & editing. **Joachim F.R. Van Guyse:** Conceptualization, Investigation, Writing - review & editing. **Ali Tigrine:** Investigation. **Maarten Vergaelen:** Investigation. **Richard Hoogenboom:** Conceptualization, Methodology, Writing - review & editing, Supervision. **Karen De Clerck:** Conceptualization, Methodology, Writing - review & editing, Supervision.

Declaration of competing interest

The authors declare that they have no known competing financial interests or personal relationships that could have appeared to influence the work reported in this paper.

Acknowledgement

This work was supported by the Fonds voor Wetenschappelijk Onderzoek (FWO, Belgium) with two Strategic Basic Research grants [1S05517N, 2017] of ES and [1S89118N, 2018] of JB. Furthermore, KDC and RH would like to thank continued support from Ghent University and FWO.

Data availability

The raw data required to reproduce these findings cannot be shared at this time due to technical or time limitations. The processed data required to reproduce these findings are available in Supporting Information.

References

[1] M. Glassner, M. Vergaelen, R. Hoogenboom, Poly(2-oxazoline)s: a comprehensive overview of polymer structures and their physical properties, Polym. Int. 67 (2018) 32–45, https://doi.org/10.1002/pi.5457.
[2] N. Adams, U.S. Schubert, Poly(2-oxazolines) in biological and biomedical application contexts, Adv. Drug Deliv. Rev. 59 (2007) 1504–1520, https://doi.org/10.1016/j.addr.2007.08.018.
[3] D. Pizzi, J. Humphries, J.P. Morrow, N.L. Fletcher, C.A. Bell, K.J. Thurecht, et al., Poly(2-oxazoline) macromonomers as building blocks for functional and biocompatible polymer architectures, Eur. Polym. J. 121 (2019), 109258. https://doi.org/10.1016/J.EURPOLYMJ.2019.109258.
[4] T. Lorson, M.M. Lübtow, E. Wegener, M.S. Haider, S. Borova, D. Nahm, et al., Poly(2-oxazoline)s based biomaterials: a comprehensive and critical update, Biomaterials 178 (2018) 204–280, https://doi.org/10.1016/J.BIOMATERIALS.2018.05.022.
[5] M. Grube, M.N. Leiske, U.S. Schubert, I. Nischang, POx as an alternative to PEG? A hydrodynamic and light scattering study, Macromolecules 51 (2018) 1905–1916, https://doi.org/10.1021/acs.macromol.7b02665.
[6] L. Benski, J.C. Tiller, Telechelic biocidal poly(2-oxazoline)s and polycations, Eur. Polym. J. 120 (2019), 109233. https://doi.org/10.1016/J.EURPOLYMJ.2019.109233.
[7] T.X. Viegas, Z. Fang, K. Yoon, R. Weimer, B. Dizman, Poly(oxazolines), Eng. Biomater. Drug Deliv. Syst. Beyond Polyethyl. Glycol, Woodhead Publishing 2018, pp. 173–198, https://doi.org/10.1016/B978-0-08-101750-0.00006-4.

[8] R. Luxenhofer, Y. Han, A. Schulz, J. Tong, Z. He, A.V. Kabanov, et al., Poly(2-oxazoline)s as polymer therapeutics, Macromol. Rapid Commun. 33 (2012) 1613–1631, https://doi.org/10.1002/marc.201200354.

[9] R. Luxenhofer, R. Jordan, Click chemistry with poly(2-oxazoline)s, Macromolecules 39 (2006) 3509–3516, https://doi.org/10.1021/ma052515m.

[10] K. Lava, B. Verbraeken, R. Hoogenboom, Poly(2-oxazoline)s and click chemistry: a versatile toolbox toward multi-functional polymers, Eur. Polym. J. 65 (2015) 98–111, https://doi.org/10.1016/j.eurpolymj.2015.01.014.

[11] G. Delaittre, Telechelic poly(2-oxazoline)s, Eur. Polym. J. (2019), 109281. https://doi.org/10.1016/J.EURPOLYMJ.2019.109281.

[12] B.A. Drain, C.R. Becer, Synthetic approaches on conjugation of poly(2-oxazoline)s with vinyl based polymers, Eur. Polym. J. 119 (2019) 344–351, https://doi.org/10.1016/J.EURPOLYMJ.2019.07.047.

[13] J.F.R. Van Guyse, M.A. Mees, M. Vergaelen, M. Baert, B. Verbraeken, P.J. Martens, et al., Amidation of methyl ester side chain bearing poly(2-oxazoline)s with tyramine: a quest for a selective and quantitative approach, Polym. Chem. 10 (2019) 954–962, https://doi.org/10.1039/C9PY00014C.

[14] H.M.L. Lambermont-Thijs, H.P.C. van Kuringen, J.P.W. van der Put, U.S. Schubert, R. Hoogenboom, Temperature induced solubility transitions of various poly(2-oxazoline)s in ethanol-water solvent mixtures, Polymers (Basel) 2 (2010) 188–199, https://doi.org/10.3390/polym2030188.

[15] J.S. Park, K. Kataoka, Comprehensive and accurate control of thermosensitivity of poly(2-alkyl-2-oxazoline)s via well-defined gradient or random copolymerization, Macromolecules 40 (2007) 3599–3609, https://doi.org/10.1021/ma0701181.

[16] M.A. Boerman, H.L. Van der Laan, J.C.M.E. Bender, R. Hoogenboom, J.A. Jansen, S.C. Leeuwenburgh, et al., Synthesis of pH- and thermoresponsive poly(2-n-propyl-2-oxazoline) based copolymers, J. Polym. Sci. Part A Polym. Chem. 54 (2016) 1573–1582, https://doi.org/10.1002/pola.28011.

[17] N. Oleszko-Torbus, A. Utrata-Wesołek, W. Wałach, A. Dworak, Solution behavior of thermoresponsive random and gradient copolymers of 2-n-propyl-2-oxazoline, Eur. Polym. J. 88 (2017) 613–622, https://doi.org/10.1016/J.EURPOLYMJ.2016.11.008.

[18] S. Huber, R. Jordan, Modulation of the lower critical solution temperature of 2-alkyl-2-oxazoline copolymers, Colloid Polym. Sci. 286 (2008) 395–402, https://doi.org/10.1007/s00396-007-1781-y.

[19] D. Menne, F. Pitsch, J.E. Wong, A. Pich, M. Wessling, Temperature-modulated water filtration using microgel-functionalized hollow-fiber membranes, Angew. Chem. Int. Ed. 53 (2014) 5706–5710, https://doi.org/10.1002/anie.201400316.

[20] S. Darvishmanesh, X. Qian, S.R. Wickramasinghe, Responsive membranes for advanced separations, Curr. Opin. Chem. Eng. 8 (2015) 98–104, https://doi.org/10.1016/J.COCHE.2015.04.002.

[21] Y. Park, M.P. Gutierrez, L.P. Lee, Reversible self-actuated thermo-responsive pore membrane, Sci. Rep. 6 (2016), 39402. https://doi.org/10.1038/srep39402.

[22] H. Kim, K. Kim, S.J. Lee, Nature-inspired thermo-responsive multifunctional membrane adaptively hybridized with PNIPAm and PPy, NPG Asia Mater. 9 (2017) e445, https://doi.org/10.1038/am.2017.168.

[23] J. Anu Bhushani, C. Anandharamakrishnan, Electrospinning and electrospraying techniques: potential food based applications, Trends Food Sci. Technol. 38 (2014) 21–33, https://doi.org/10.1016/J.TIFS.2014.03.004.

[24] T. Amna, J. Yang, K.-S. Ryu, I.H. Hwang, Electrospun antimicrobial hybrid mats: innovative packaging material for meat and meat-products, J. Food Sci. Technol. 52 (2015) 4600–4606, https://doi.org/10.1007/s13197-014-1508-2.

[25] M. Noruzi, Electrospun nanofibres in agriculture and the food industry: a review, J. Sci. Food Agric. 96 (2016) 4663–4678, https://doi.org/10.1002/jsfa.7737.

[26] A. Macagnano, E. Zampetti, E. Kny (Eds.), Electrospinning for High Performance Sensors, Springer International Publishing, Cham, 2015https://doi.org/10.1007/978-3-319-14406-1.

[27] J.H. Wendorff, S. Agarwal, A. Greiner, Electrospinning: Materials, Processing, and Applications, John Wiley & Sons, 2012.

[28] D. Pisignano, Polymer Nanofibers: Building Blocks for Nanotechnology, 2013.

[29] L.A. Andrady, Science and Technology of Polymer Nanofibers, 2008.

[30] S. Ramakrishna, K. Fujihara, W.-E. Teo, T.-C. Lim, Z. Ma, An Introduction to Electrospinning and Nanofibers, World Scientific, 2005.

[31] L. Persano, A. Camposeo, C. Tekmen, D. Pisignano, Industrial upscaling of electrospinning and applications of polymer nanofibers: a review, Macromol. Mater. Eng. 298 (2013) 504–520, https://doi.org/10.1002/mame.201200290.

[32] T. Subbiah, G.S. Bhat, R.W. Tock, S. Parameswaran, S.S. Ramkumar, Electrospinning of nanofibers, J. Appl. Polym. Sci. 96 (2005) 557–569, https://doi.org/10.1002/app.21481.

[33] B. Stubbe, Y. Li, M. Vergaelen, S. Van Vlierberghe, P. Dubruel, K. De Clerck, et al., Aqueous electrospinning of poly(2-ethyl-2-oxazoline): mapping the parameter space, Eur. Polym. J. 88 (2017) 724–732, https://doi.org/10.1016/J.EURPOLYMJ.2016.09.014.

[34] Y. Li, M. Vergaelen, E. Schoolaert, R. Hoogenboom, K. De Clerck, Effect of crosslinking stage on photocrosslinking of benzophenone functionalized poly(2-ethyl-2-oxazoline) nanofibers obtained by aqueous electrospinning, Eur. Polym. J. 112 (2019) 24–30, https://doi.org/10.1016/j.eurpolymj.2018.12.030.

[35] Y. Li, M. Vergaelen, X. Pan, F.E. Du Prez, R. Hoogenboom, K. De Clerck, In situ crosslinked nanofibers by aqueous electrospinning of selenol-functionalized poly(2-oxazoline)s, Macromolecules 51 (2018) 6149–6156, https://doi.org/10.1021/acs.macromol.8b01113.

[36] W. Wałach, N. Oleszko-Torbus, A. Utrata-Wesołek, M. Bochenek, E. Kijeńska-Gawrońska, Ż. Górecka, et al., Processing of (co)poly(2-oxazoline)s by electrospinning and extrusion from melt and the postprocessing properties of the (co)polymers, Polymers (Basel) 12 (2020) 295, https://doi.org/10.3390/polym12020295.

[37] L. Buruaga, A. Gonzalez, J.J. Iruin, Electrospinning of poly (2-ethyl-2-oxazoline), J. Mater. Sci. 44 (2009) 3186–3191, https://doi.org/10.1007/s10853-009-3424-9.

[38] G. Paramasivam, M. Vergaelen, M.-R. Ganesh, R. Hoogenboom, A. Sundaramurthy, Hydrogen bonded capsules by layer-by-layer assembly of tannic acid and poly(2-n-propyl-2-oxazoline) for encapsulation and release of macromolecules, J. Mater. Chem. B 5 (2017) 8967–8974, https://doi.org/10.1039/C7TB02284K.

[39] I. Erel, H. Schlaad, A.L. Demirel, Effect of structural isomerism and polymer end group on the pH-stability of hydrogen-bonded multilayers, J. Colloid Interface Sci. 361 (2011) 477–482, https://doi.org/10.1016/J.JCIS.2011.05.033.

[40] S. Hendessi, P. Tatar Güner, A. Miko, A.L. Demirel, Hydrogen bonded multilayers of poly(2-ethyl-2-oxazoline) stabilized silver nanoparticles and tannic acid, Eur. Polym. J. 88 (2017) 666–678, https://doi.org/10.1016/J.EURPOLYMJ.2016.10.039.

[41] M. Haktaniyan, S. Atilla, E. Cagli, I. Erel-Goktepe, pH- and temperature-induced release of doxorubicin from multilayers of poly(2-isopropyl-2-oxazoline) and tannic acid, Polym. Int. 66 (2017) 1851–1863, https://doi.org/10.1002/pi.5458.

[42] J.L. Whittaker, S. Subianto, N.K. Dutta, N.R. Choudhury, Induced insolubility of electrospun poly(N-vinylcaprolactam) fibres through hydrogen bonding with tannic acid, Polym. (United Kingdom). 87 (2016) 194–201, https://doi.org/10.1016/j.polymer.2016.01.072.

[43] E.B. Adatoz, S. Hendessi, C.W. Ow-Yang, A.L. Demirel, Restructuring of poly(2-ethyl-2-oxazoline)/tannic acid multilayers into fibers, Soft Matter 14 (2018) 3849–3857, https://doi.org/10.1039/C8SM00381E.

[44] E.J. Falde, S.T. Yohe, Y.L. Colson, M.W. Grinstaff, Superhydrophobic materials for biomedical applications, Biomaterials 104 (2016) 87–103, https://doi.org/10.1016/J.BIOMATERIALS.2016.06.050.

[45] Y.Y. Yan, N. Gao, W. Barthlott, Mimicking natural superhydrophobic surfaces and grasping the wetting process: a review on recent progress in preparing superhydrophobic surfaces, Adv. Colloid Interf. Sci. 169 (2011) 80–105, https://doi.org/10.1016/J.CIS.2011.08.005.

[46] E. Loccufier, J. Geltmeyer, L. Daelemans, D.R. D'hooge, K. De Buysser, K. De Clerck, Silica nanofibrous membranes for the separation of heterogeneous azeotropes, Adv. Funct. Mater. 28 (2018), 1804138. https://doi.org/10.1002/adfm.201804138.

[47] I. Sas, R.E. Gorga, J.A. Joines, K.A. Thoney, Literature review on superhydrophobic self-cleaning surfaces produced by electrospinning, J. Polym. Sci. Part B Polym. Phys. 50 (2012) 824–845, https://doi.org/10.1002/polb.23070.

[48] W.S.Y. Wong, P. Gutruf, S. Sriram, M. Bhaskaran, Z. Wang, A. Tricoli, Strain engineering of wave-like nanofibers for dynamically switchable adhesive/repulsive surfaces, Adv. Funct. Mater. 26 (2016) 399–407, https://doi.org/10.1002/adfm.201503982.

[49] P. Tian, Z. Guo, Bioinspired silica-based superhydrophobic materials, Appl. Surf. Sci. 426 (2017) 1–18, https://doi.org/10.1016/J.APSUSC.2017.07.134.

[50] S. Varagnolo, F. Raccanello, M. Pierno, G. Mistura, M. Moffa, L. Persano, et al., Highly sticky surfaces made by electrospun polymer nanofibers, RSC Adv. 7 (2017) 5836–5842, https://doi.org/10.1039/c6ra24922a.

[51] X. Wang, B. Ding, J. Yu, M. Wang, Engineering biomimetic superhydrophobic surfaces of electrospun nanomaterials, Nano Today 6 (2011) 510–530, https://doi.org/10.1016/j.nantod.2011.08.004.

[52] N. Nuraje, W.S. Khan, Y. Lei, M. Ceylan, R. Asmatulu, Superhydrophobic electrospun nanofibers, J. Mater. Chem. A 1 (2013) 1929–1946, https://doi.org/10.1039/C2TA00189F.

[53] X. Lu, J. Zhou, Y. Zhao, Y. Qiu, J. Li, Room temperature ionic liquid based polystyrene nanofibers with superhydrophobicity and conductivity produced by electrospinning, Chem. Mater. 20 (2008) 3420–3424, https://doi.org/10.1021/cm800045h.

[54] B.D. Monnery, V.V. Jerca, O. Sedlacek, B. Verbraeken, R. Cavill, R. Hoogenboom, Defined high molar mass poly(2-oxazoline)s, Angew. Chemie - Int. Ed. 57 (2018) 15400–15404, https://doi.org/10.1002/anie.201807796.

[55] B. Verbraeken, B.D. Monnery, K. Lava, R. Hoogenboom, The chemistry of poly(2-oxazoline)s, Encycl. Polym. Sci. Technol, John Wiley & Sons, Inc, Hoboken, NJ, USA 2018, pp. 1–59, https://doi.org/10.1002/0471440264.pst626.pub2.

[56] H. Goossens, S. Catak, M. Glassner, V.R. De La Rosa, B.D. Monnery, F. De Proft, et al., Cationic ring-opening polymerization of 2-propyl-2-oxazolines: understanding structural effects on polymerization behavior based on molecular modeling, ACS Macro Lett. 2 (2013) 651–654, https://doi.org/10.1021/mz400293y.

[57] Q. Zhang, C. Weber, U.S. Schubert, R. Hoogenboom, Thermoresponsive polymers with lower critical solution temperature: from fundamental aspects and measuring techniques to recommended turbidimetry conditions, Mater. Horiz. 4 (2017) 109–116, https://doi.org/10.1039/C7MH00016B.

[58] M.W. Lee, S. An, S.S. Latthe, C. Lee, S. Hong, S.S. Yoon, Electrospun polystyrene nanofiber membrane with superhydrophobicity and superoleophilicity for selective separation of water and low viscous oil, ACS Appl. Mater. Interfaces 5 (2013) 10597–10604, https://doi.org/10.1021/am404156k.

[59] R. Asmatulu, M. Ceylan, N. Nuraje, Study of superhydrophobic electrospun nanocomposite fibers for energy systems, Langmuir 27 (2011) 504–507, https://doi.org/10.1021/la103661c.

[60] A.B.D. Cassie, S. Baxter, Wettability of porous surfaces, Trans. Faraday Soc. 40 (1944) 546, https://doi.org/10.1039/tf9444000546.

[61] R.J. Crawford, E.P. Ivanova, Superhydrophobic Surfaces, Elsevier, 2015https://doi.org/10.1016/C2013-0-13636-7.

[62] M.M. Bloksma, D.J. Bakker, C. Weber, R. Hoogenboom, U.S. Schubert, The effect of hofmeister salts on the LCST transition of poly(2-oxazoline)s with varying hydrophilicity, Macromol. Rapid Commun. 31 (2010) 724–728, https://doi.org/10.1002/marc.200900843.

[63] A. Sundaramurthy, M. Vergaelen, S. Maji, R. Auzély-Velty, Z. Zhang, B.G. De Geest, et al., Hydrogen bonded multilayer films based on poly(2-oxazoline)s and tannic acid, Adv. Healthc. Mater. 3 (2014) 2040–2047, https://doi.org/10.1002/adhm.201400377.

[64] E.F.-J. Rettler, M.V. Unger, R. Hoogenboom, H.W. Siesler, U.S. Schubert, Water uptake of poly(2-N-alkyl-2-oxazoline)s: temperature-dependent Fourier transform infrared (FT-IR) spectroscopy and two-dimensional correlation analysis (2DCOS), Appl. Spectrosc. 66 (2012) 1145–1155, https://doi.org/10.1366/12-06650.
[65] I. Erel-Unal, S.A. Sukhishvili, Hydrogen-bonded multilayers of a neutral polymer and a polyphenol, Macromolecules 41 (2008) 3962–3970, https://doi.org/10.1021/ma800186q.
[66] T. Shutava, M. Prouty, D. Kommireddy, Y. Lvov, pH responsive decomposable layer-by-layer nanofilms and capsules on the basis of tannic acid, Macromolecules 38 (2005) 2850–2858, https://doi.org/10.1021/ma047629x.
[67] A. Barbasz, M. Oćwieja, J. Barbasz, Cytotoxic activity of highly purified silver nanoparticles sol against cells of human immune system, Appl. Biochem. Biotechnol. 176 (2015) 817–834, https://doi.org/10.1007/s12010-015-1613-3.
[68] G. Socrates, Infrared and Raman Characteristic Group Frequencies, John Wiley & Sons, 2004https://doi.org/10.1002/jrs.1238.
[69] B.C. Smith, Infrared Spectral Interpretation: A Systematic Approach, CRC Press, 1998https://doi.org/10.1017/CBO9781107415324.004.
[70] C. Wang, Y. Li, Y. Ma, Y. Gao, D. Dong, J. Fang, et al., Thermoresponsive polymeric nanoparticles based on poly(2-oxazoline)s and tannic acid, J. Polym. Sci. Part A Polym. Chem. 56 (2018) 1520–1527, https://doi.org/10.1002/pola.29033.
[71] H. Fan, L. Wang, X. Feng, Y. Bu, D. Wu, Z. Jin, Supramolecular hydrogel formation based on tannic acid, Macromolecules 50 (2017) 666–676, https://doi.org/10.1021/acs.macromol.6b02106.
[72] M.A. Pantoja-Castro, H. González-Rodríguez, Study by infrared spectroscopy and thermogravimetric analysis of tannins and tannic acid, Rev. Latinoam. Química. 39 (2012) 107–112.
[73] B. Zhou, X. Hu, J. Zhu, Z. Wang, X. Wang, M. Wang, Release properties of tannic acid from hydrogen bond driven antioxidative cellulose nanofibrous films, Int. J. Biol. Macromol. 91 (2016) 68–74, https://doi.org/10.1016/j.ijbiomac.2016.05.084.
[74] C. Ronco, W.R. Clark, Haemodialysis membranes, Nat. Rev. Nephrol. 14 (2018) 394–410, https://doi.org/10.1038/s41581-018-0002-x.
[75] L. Huang, N.-N. Bui, M.T. Meyering, T.J. Hamlin, J.R. McCutcheon, Novel hydrophilic nylon 6,6 microfiltration membrane supported thin film composite membranes for engineered osmosis, J. Membr. Sci. 437 (2013) 141–149, https://doi.org/10.1016/J.MEMSCI.2013.01.046.
[76] J.T. Arena, B. McCloskey, B.D. Freeman, J.R. McCutcheon, Surface modification of thin film composite membrane support layers with polydopamine: enabling use of reverse osmosis membranes in pressure retarded osmosis, J. Membr. Sci. 375 (2011) 55–62, https://doi.org/10.1016/J.MEMSCI.2011.01.060.
[77] J.R. McCutcheon, M. Elimelech, Influence of membrane support layer hydrophobicity on water flux in osmotically driven membrane processes, J. Membr. Sci. 318 (2008) 458–466, https://doi.org/10.1016/J.MEMSCI.2008.03.021.
[78] L. Huang, J.T. Arena, S.S. Manickam, X. Jiang, B.G. Willis, J.R. McCutcheon, Improved mechanical properties and hydrophilicity of electrospun nanofiber membranes for filtration applications by dopamine modification, J. Membr. Sci. 460 (2014) 241–249, https://doi.org/10.1016/J.MEMSCI.2014.01.045.
[79] Y. Huang, J. Song, C. Yang, Y. Long, H. Wu, Scalable manufacturing and applications of nanofibers, Mater. Today 28 (2019) 98–113, https://doi.org/10.1016/J.MATTOD.2019.04.018.
[80] B. Bhushan, M. Nosonovsky, The rose petal effect and the modes of superhydrophobicity, Philos. Trans. A Math. Phys. Eng. Sci. 368 (2010) 4713–4728, https://doi.org/10.1098/rsta.2010.0203.
[81] L. Feng, Y. Zhang, J. Xi, Y. Zhu, N. Wang, F. Xia, et al., Petal effect: a superhydrophobic state with high adhesive force, Langmuir 24 (2008) 4114–4119, https://doi.org/10.1021/la703821h.
[82] C.R. Szczepanski, F. Guittard, T. Darmanin, Recent advances in the study and design of parahydrophobic surfaces: from natural examples to synthetic approaches, Adv. Colloid Interf. Sci. 241 (2017) 37–61, https://doi.org/10.1016/J.CIS.2017.01.002.
[83] A.M. Nicolini, C.F. Fronczek, J.Y. Yoon, Droplet-based immunoassay on a “sticky” nanofibrous surface for multiplexed and dual detection of bacteria using smartphones, Biosens. Bioelectron. 67 (2015) 560–569, https://doi.org/10.1016/j.bios.2014.09.040.
[84] W.S.Y. Wong, N. Nasiri, G. Liu, N. Rumsey-Hill, V.S.J. Craig, D.R. Nisbet, et al., Flexible transparent hierarchical nanomesh for rose petal-like droplet manipulation and lossless transfer, Adv. Mater. Interfaces 2 (2015), 1500071. https://doi.org/10.1002/admi.201500071.
[85] F. Zheng, H. Deng, X. Zhao, X. Li, C. Yang, Y. Yang, et al., Fluorinated hyperbranched polyurethane electrospun nanofibrous membrane: fluorine-enriching surface and superhydrophobic state with high adhesion to water, J. Colloid Interface Sci. 421 (2014) 49–55, https://doi.org/10.1016/j.jcis.2014.01.009.